

PROBING HIGH-REDSHIFT DISKS WITH DAMPED Ly α SYSTEMS

ARTHUR M. WOLFE

University of California, San Diego, CASS, La Jolla, CA 92093-0424

Abstract. Evidence is presented that the damped Ly α absorption systems are the high-redshift ($z > 3$) progenitors of galaxy disks. I discuss kinematic evidence that the damped Ly α systems are rotating disks. I also discuss implications of the lack of metal-poor damped Ly α systems with line width $\Delta v > 100 \text{ km s}^{-1}$. I then present new evidence stemming from correlations between element-abundance ratios and [Fe/H], which connects damped systems to the thick stellar disk of the Galaxy. I discuss the connections between damped Ly α systems and Lyman break galaxies, and how [CII] 158 μm emission from damped Ly α systems discriminates among competing theories of galaxy formation.

1. Introduction

When did the disks of ordinary galaxies form? This is the central question to be addressed in my talk. At this meeting, evidence was presented suggesting the *bulk* of the disk population was in place by $z \approx 1$. While mergers between disks and infall of gas onto disks undoubtedly occur subsequently, the surveys by Ellis, Lilly, and Faber all rule out substantial changes in the stellar content of disks since $z = 1$. Further evidence against significant changes in the disk populations comes from the Galaxy. From her studies of stars in the thick disk, Wyse (this volume) concluded that the Galaxy has not undergone a major merger during the past 12 Gyr. Provided the Galaxy is typical, this adds strong support to the idea that disks, in this case the thick disk, were in place *before* $z = 1$.

How long before? This question is crucial since hierarchical cosmologies predict that only a small fraction of current disk galaxies were in place by $z \approx 3$. Rather, CDM models predict the bulk of the protogalactic mass distribution to be in low-mass subgalactic progenitors at these redshifts. This is a generic property of CDM cosmologies, and one that should be tested.

In my talk I will describe observations that not only test hierarchical theories of galaxy formation, but also probe the nature of the protogalactic mass distribution. The work centers on the damped Ly α systems, because of compelling evidence that these H I layers supply the baryons comprising visible stars in current galaxies (cf. Storrie-Lombardi & Wolfe 2000). Therefore, my talk focuses on gas rather than stars (but see § 4). Gas provides a more accurate picture of the baryonic content of protogalaxies because most of the baryons at high z were gas.

2. Kinematics: The Case for Rotation

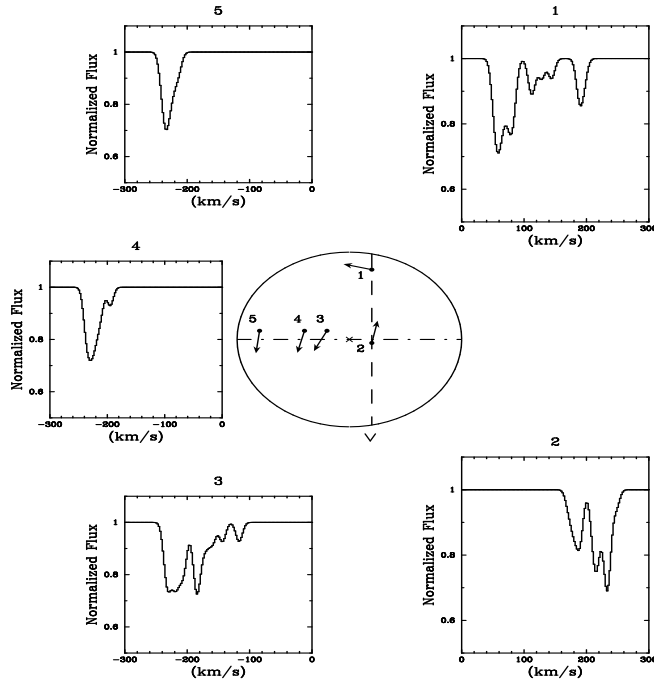


Figure 1. “Edge-leading” velocity profiles produced by rotating disks (Fig. 3 in Prochaska & Wolfe 1997). Circle is counter-clockwise rotating disk with $V_{rot} = 250 \text{ km s}^{-1}$. Dots are intersection points between sightlines and midplane of disk. Vertical dashed line is sightline for intersection points 1 and 2, and horizontal line is kinematic major axis. Absorption profiles produced at indicated locations

The evidence for rotating disks stems from accurate velocity profiles of metal lines that J. X. Prochaska and I have acquired with HIRES, the echelle spectrograph on the Keck I telescope. Along with profiles kindly supplied by W. L. W. Sargent, we have acquired accurate profiles for low-ions such as Fe^+ and Si^+ for over 40 high- z damped $\text{Ly}\alpha$ systems. Low ions are crucial as they trace the neutral gas which gives rise to damped $\text{Ly}\alpha$ lines.

The velocity profiles (see Wolfe 1999; Prochaska & Wolfe 1997) consist of multiple narrow-velocity components spanning velocity intervals Δv between 20 and 290 km s^{-1} . The components are not randomly distributed in velocity space. Rather, the component with the largest optical depth is at the profile edge in 75 % of the profiles with $\Delta v > 40 \text{ km s}^{-1}$. The most straightforward explanation for this “edge leading” asymmetry is that the damped $\text{Ly}\alpha$ sightlines traverse rotating disks in which the density of absorbing clouds decreases exponentially in the radial and vertical directions with scale lengths R_d and h (Prochaska & Wolfe 1997). Figure 1 shows how “edge-leading” profiles naturally arise from randomly selected impact parameters. The figure also shows why Δv decreases with increasing impact parameter. While other mechanisms have been suggested

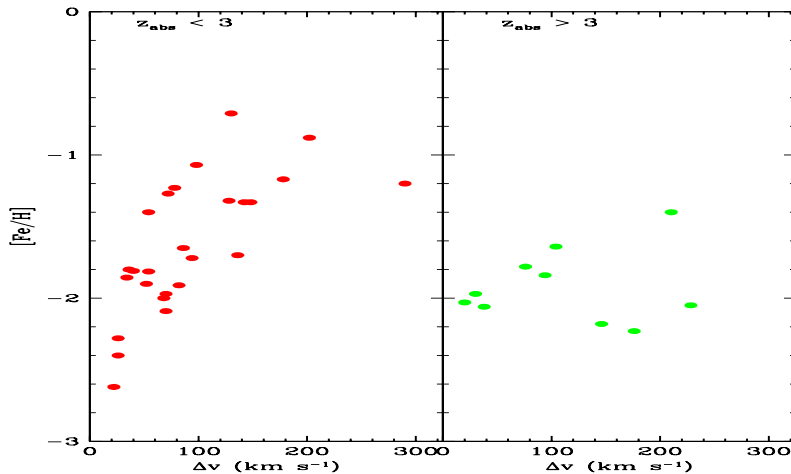


Figure 2. $[\text{Fe}/\text{H}]$ versus Δv for damped $\text{Ly}\alpha$ systems at (a) $z < 3$ and (b) $z > 3$, where $[\text{Fe}/\text{H}] = \log(\text{Fe}/\text{H}) - \log(\text{Fe}/\text{H})_{\odot}$

to explain the profile asymmetries (e.g. Haehnelt et al. 1997), exponential rotating disks provide the most straightforward explanation.

Using Monte Carlo techniques, we tested the semi-analytic models of Mo et al. (1998) in which centrifugally-supported disks are at the centers of dark-matter halos with mass distribution determined by Press-Schechter functions and CDM power spectra. We generated synthetic velocity profiles by letting randomly selected sightlines traverse randomly-oriented exponential disks with rotation speeds V_{rot} equal to $\sqrt{GM(r)/r}$ at the virial radius. We found the Δv predicted by single-disk CDM models cannot account for the significant fraction of Δv between 100 and 300 km s^{-1} , since the median V_{rot} predicted by single-disk CDM models are less than 100 km s^{-1} . However, the TF model in which the input distribution of V_{rot} at high redshift is determined by the Tully-Fisher relation and the Schechter luminosity function is compatible with the data owing to the larger fraction of disks $V_{rot} > 100 \text{ km s}^{-1}$ (Wolfe & Prochaska 2000). Thick disks with $h \approx 0.3R_d$ are required to obtain $\Delta v > 100 \text{ km s}^{-1}$.

3. Metals in Damped $\text{Ly}\alpha$ Systems

3.1. Metallicity versus Kinematics in Damped $\text{Ly}\alpha$ Systems

We also used the HIRES velocity profiles to determine the metallicities of damped $\text{Ly}\alpha$ systems (Prochaska & Wolfe 2000). Combining metallicity and kinematic information we find a phenomenon that bears upon the presence of rotating disks at high redshifts. And this is the clear deficit at $z < 3$ of metal-poor systems with $\Delta v > 100 \text{ km s}^{-1}$ shown in Figure 2a. The absence of these systems is real and not an artifact due to selection effects. This is indicated by the presence of such systems in the $z > 3$ sample (Fig. 2b). Moreover, dust would lead to the absence of metal-rich rather than metal-poor systems. The enlarged sample of $[\text{Fe}/\text{H}]$ abundances strengthens the case first made with a smaller sample of $[\text{Zn}/\text{H}]$, Δv pairs (Wolfe & Prochaska 1998). We interpret

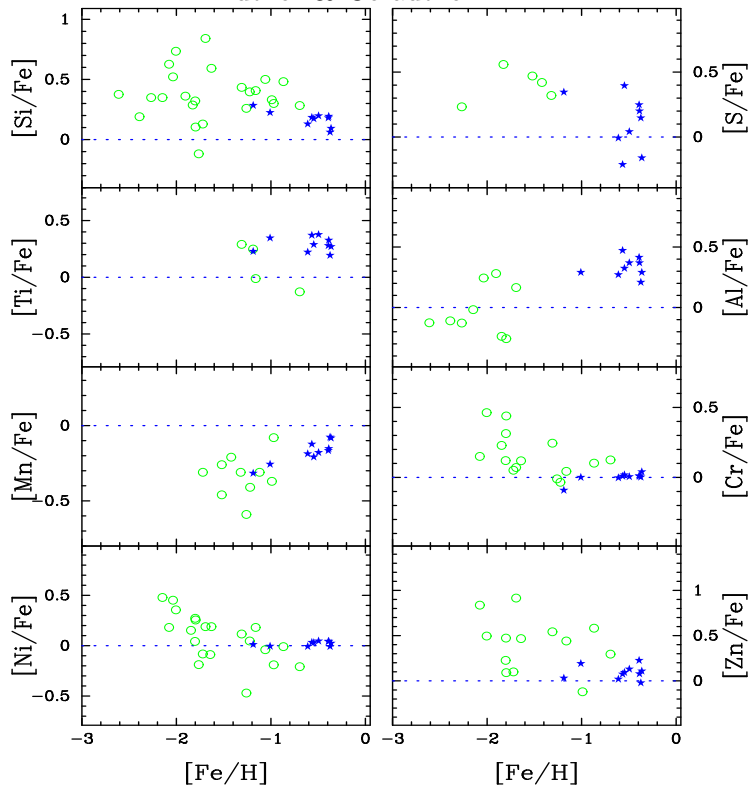


Figure 3. Abundance ratios versus $[\text{Fe}/\text{H}]$ for damped systems (circles) and thick disk stars (stars) (from Prochaska et al. 2000)

this effect to arise from negative radial gradients in $[\text{Fe}/\text{H}]$ in rotating disks. High $[\text{Fe}/\text{H}]$ are required at small radii because low impact parameters, b , are a necessary condition for large Δv (see Fig. 1). We find a wider distribution of b contributes to systems with smaller Δv . Thus, at small Δv , the lower $[\text{Fe}/\text{H}]$ come from low $[\text{Fe}/\text{H}]$ at large radii, while higher $[\text{Fe}/\text{H}]$ again come from small b but in disks that are more face-on. *Therefore, the increase in scatter of $[\text{Fe}/\text{H}]$ with decreasing Δv is naturally produced by the rotating disk models.* However, since variations in metallicity in nearby spirals rarely span more than 1 dex, a positive correlation between $[\text{Fe}/\text{H}]$ and M would help to explain the full effect.

3.2. Abundance Patterns and the Thick Disk Connection

Figure 3 plots abundance ratios of various elements versus $[\text{Fe}/\text{H}]$ for damped Ly α systems and stars in the Galaxy thick disk. Comparison with the thick disk is motivated by the large vertical scale-heights required in our model gaseous disks, since this raises the possibility that high- z damped Ly α systems are the progenitors of thick stellar disks. To demonstrate the plausibility of this hypothesis, we showed that the metal-rich damped Ly α systems contain sufficient baryons at mean metallicity, $\langle [\text{Fe}/\text{H}] \rangle = -0.6$, to account for the the mass content and metallicity of thick disks (Wolfe & Prochaska 1998). Here I discuss further evidence in support of this idea.

The abundances in Figure 3 were inferred from HIRES data obtained for a kinematically selected sample of stars in the thick disk and our sample of damped Ly α systems. The stellar atmospheres programs used to deduce the thick disk abundances are described in Prochaska et al. (2000). The figure plots results for α , Fe peak, and light elements. As [Fe/H] increases we find tentative evidence that [X/Fe] for the damped systems evolves toward [X/Fe] for the thick disk when X = Si, Zn, and Mn. The results are especially striking for [Mn/Fe]. We find two possible interpretations for these trends. The first is a nucleosynthetic explanation. Lu et al. (1996) argued that the damped systems exhibit classic type II Sn patterns with enhanced [α /Fe] ratios, deficient [Mn/Fe] ratios (due to the odd-even effect), and unpeculiar [Cr/Fe] and [Ni/Fe] ratios. The problem with this argument was that [Zn/Fe] = 0 in stars with a wide range in metallicities; whereas [Zn/Fe] \approx 0.3 in damped systems. With our more accurate spectroscopy we find [Zn/Fe] = 0.1 in thick-disk stars where [Fe/H] = -0.6. And there is tentative evidence that [Zn/Fe] is higher for thick-disk stars with lower [Fe/H]. That Zn does not track Fe is not surprising since recent calculations indicate Zn is not produced in the same type I Sn responsible for most of the Fe. Rather, Zn may be produced in neutrino-driven winds in type II Sn (Hoffman 1996). Therefore, it is likely that the [Zn/Fe] ratio in damped Ly α systems is partially nucleosynthetic in origin. On the other hand, Pettini et al. (1997) argued that the abundance patterns in damped systems are caused by depletion of heavy elements on to dust grains. This is consistent with all the observed patterns except for [Mn/Fe] and possibly [Ti/Fe]. The strongest argument in favor of this explanation was the high [Zn/Fe] ratio. But we have shown that part of this ratio probably originates from nucleosynthesis, and so a more likely explanation is that the damped Ly α abundance pattern results from small amount of dust superposed on a type II Sn abundance pattern.

As a result, we conjecture that metal-poor damped Ly α systems evolve into metal-rich objects that become thick stellar disks at high redshifts, say $z \approx 3$. Since the velocity dispersion of the model gaseous disks, $\sigma \approx 10 \text{ km s}^{-1}$, subsequent merger events are required to heat the stars to the observed velocity dispersion of the thick disk, $\sigma \approx 40 \text{ km s}^{-1}$. In that sense our model does not differ substantially from the scenario put forward by Wyse (these proceedings).

4. Connecting Lyman Break Galaxies to Damped Ly α Systems

For the past two years, our group (Gawiser, Prochaska, Cooke, & Wolfe) has been searching for Lyman break galaxies in fields centered on quasars with foreground damped Ly α systems. Our goals are to (i) find galaxies physically associated with the damped systems, and (ii) determine how often the damped Ly α redshifts coincide with the redshift spikes characterizing the distribution of known Lyman break galaxies (Steidel 1999). The correlation between damped systems and Lyman break galaxies is very interesting because it tells us about the bias of the damped Ly α galaxies, and, as a result, about their mass. Stated differently, if damped Ly α redshifts are preferentially located in Lyman break redshift spikes, this would mean the amplitudes of density fluctuations, $(\delta\rho/\rho)_{DLA}$, destined to become damped Ly α galaxies are too low to collapse and form galaxies unless they are boosted by the enhanced mass density provided by the Lyman

break clusters. This would indicate higher-than-typical masses given the nature of the power spectrum.

Our survey initially focused on B drop outs as there is no U band photometry currently available on the Keck telescopes. This restricted the sample to damped Ly α systems with $z = (3.8, 4.5)$. We have acquired B, R, I images for about four damped Ly α fields in which the 1σ sensitivities correspond to $B \approx 29.5$, $R \approx 26.5$, and $I \approx 26.0$. As a result we are able to detect blue drop-outs down to $R \approx 26.0$. We select candidate blue drop-outs using criteria established by Steidel and then acquire multi-object spectra for about 20 candidates per setting using the LRIS multi-object spectrograph. The data have been reduced for one field containing damped systems at $z = 3.871$ and 4.072 . While there are no confirmed galaxies near the high redshift systems, we have identified four galaxies within $\Delta z = 0.02$ of the lower redshift system. That is, four out of a total of twelve identified galaxies lie within a Steidel-like redshift spike that includes the damped redshift. If future observations show this effect to be generic, then some fraction of damped systems may evolve into galaxies likely to be found in cluster environments, such as ellipticals.

5. [C II] 158 μm Emission from Damped Ly α Systems

[C II] 158 μm emission results from transitions between the $P_{3/2}^2$ and $P_{1/2}^2$ fine structure states in C^+ . It dominates cooling by the Galaxy ISM with a luminosity $L([\text{C II}]) = 5 \times 10^7 L_\odot$ (Wright et al. 1991). Significantly, most of the 158 μm emission from the ISM in the Galaxy and in other spiral galaxies where it is detected comes from the cold neutral medium (CNM) rather than the warm neutral medium, star-forming regions in spiral arms (Madden et al. 1993), or PDRs on the surfaces of molecular clouds. The last point is especially relevant for damped Ly α systems where molecules are rarely detected (cf. Lu et al. 1999).

The 158 μm luminosities of damped Ly α systems can be estimated from $N(\text{C II}^*)$, the column density of C^+ ions in the $P_{3/2}^2$ state, which is inferred from the absorption profiles of the UV transition $\text{C II}^* 1335.708$. The 158 μm luminosity per H atom is given by

$$l_c = h\nu_{21} N(\text{CII}^*) A_{21} / N(\text{HI}) \text{ergs}^{-1} \text{H}^{-1}, \quad (1)$$

where $h\nu_{21}$ is the energy of the transition and A_{21} is the coefficient for spontaneous photon emission (Lu et al. 1999). Since $L([\text{C II}]) = \langle l_c \rangle M(\text{H I}) / m_H$, where $\langle l_c \rangle$ is the density-weighted average of l_c , we can estimate the C II luminosity from damped systems provided we know the H I mass and $\langle l_c \rangle$.

In principle we can determine $\langle l_c \rangle$ from the distribution of l_c measured along individual sightlines. Figure 4 shows estimates of l_c for 11 damped Ly α systems. We also show l_c deduced for separate sightlines through the ISM and $\langle l_c \rangle$ estimated for the ISM. We compute $\langle l_c \rangle$ for the damped sample by assuming exponential disks. In that case $\langle l_c \rangle \approx l_c$ for impact parameters $b \approx 2R_d$. Our Monte Carlo simulations show that most damped sightlines have $b < (4-5) \times R_d$. As a result $\langle l_c \rangle$ corresponds to largest $(2/4.5)^2 \times 11 \approx 2-3$ values of l_c in Figure 4. We estimate $\log \langle l_c \rangle = -26.6 \pm 0.2$. While somewhat uncertain,

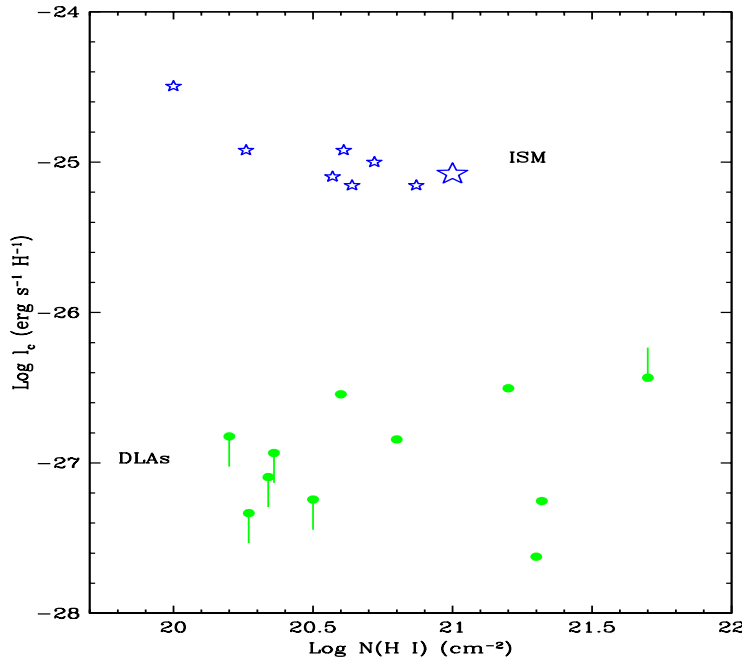


Figure 4. [CII] 158 μm emission per H atom versus $N(\text{HI})$. Circles are damped $\text{Ly}\alpha$ systems with upper limits and one lower limit shown. Small stars are estimates for separate ISM sightlines. Large star is global average of ISM from COBE

$\langle l_c \rangle$ for the damped systems is clearly more than 30 times lower than for the ISM. Since the [C II] 158 μm line is the dominant coolant for the CNM, $\langle l_c \rangle$ equals the heating rate for steady state conditions. As a result, the low value of $\langle l_c \rangle$ indicated for damped $\text{Ly}\alpha$ systems suggests low heat inputs into the protogalactic gas at high redshifts.

We also use $\langle l_c \rangle$ to compute the distribution of $L([\text{C II}])$ of damped $\text{Ly}\alpha$ systems in various cosmogonies. Mo et al. (1998) predict the fraction of intercepted damped $\text{Ly}\alpha$ systems with dark-halo masses exceeding M . We convert M to 158 μm emission noting that $L([\text{C II}]) = \langle l_c \rangle m_d M / \mu m_H$, where m_d is the fraction of dark halo mass in the disk. Assuming $\log \langle l_c \rangle = -26.5 \text{ erg s}^{-1} \text{H}^{-1}$, $\mu = 1.4$, and $m_d = 0.05$, we find $L([\text{C II}]) = 2 \times 10^7 (M / 10^{12} M_\odot) L_\odot$. We compute the flux density at a given redshift by assuming a rectangular velocity profile with width $= 2 \times V_{\text{rot}} \sin(i)$, where $\sin(i) = 0.5$. The results for the ΛCDM and TF cosmogonies are shown in Figure 5. At $z \approx 3$ the predicted ALMA detection rate is $< 3\%$ the CDM model, and about 25% in the TF model. Thus detection of [C II] 158 μm emission in high- z damped systems would be highly significant. Moreover, measurements of the velocity profile of the emitting gas could distinguish rotating disks from protogalactic clumps (Haehnelt et al. 1997).

acknowledgments I wish to thank my collaborators E. Gawiser and J. X. Prochaska for permission to quote our joint research. This work was partially supported by NSF grant AST0071257.

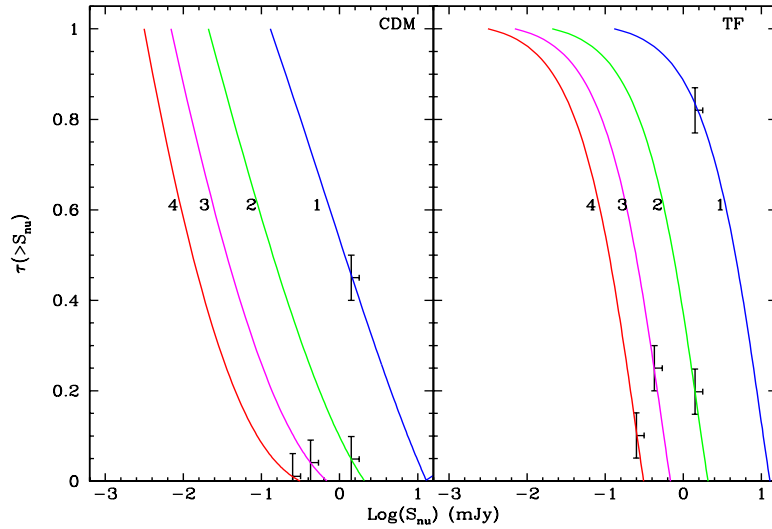


Figure 5. Fraction of damped Ly α systems detected with 158 μm flux density exceeding S_ν . (a) Curves are predictions for ΛCDM model at redshift $z = 1, 2, 3, 4$. Error bars are 3σ ALMA sensitivities for S_ν at each redshift (Brown 2000). (b) Same as (a) except for TF model

References

- Brown, R. L., 2000, private communication
- Haehnelt, M. G., Steinmetz, M., & Rauch 1998, ApJ, 495, 647
- Hoffman, R. D., et al. 1996, ApJ, 460, 478
- Lu, L., Sargent, W. L. W., Barlow, T. A., Churchill, C. C., & Vogt, S. S. 1996, ApJS, 107, 475
- Lu, L., Sargent, W. L. W., & Barlow, 1999, in Highly Redshifted Radio Lines, ed. C. L. Carilli et al., San Francisco: ASP Press, 132
- Madden, S. C. et al. 1993, ApJ 407, 579
- Mo, H.J., Mao, S., & White, S.D.M., 1998, MNRAS, 295, 319
- Pettini, M., Smith, L. J., King, D. L., & Hunstead, R. W. 1997, ApJ, 486, 655
- Prochaska, J. X., & Wolfe, A. M. 1997, ApJ 487, 73
- Prochaska, J. X., & Wolfe, A. M. 2000, ApJ 553, L5
- Prochaska, J. X., Naumov, S. L., Carney, B., McWilliam, A. & Wolfe, A. M. 2000, submitted to AJ.
- Steidel, C. C. 1999, Proc. Natl. Acad. Sci., 96, 4232
- Storrie-Lombardi, L., & Wolfe, A. M. 2000, ApJ, in press.
- Wolfe, A. M. 1999, in The Hy-Redshift Universe, ed. A. Bunker & W. van Breugel, San Francisco: ASP Press, 575.
- Wolfe, A. M., & Prochaska, J. X. 1998, ApJ, 494, L15
- Wolfe, A. M., & Prochaska, J. X. 2000, ApJ, submitted for publication
- Wright, E. L. et al. 1991, ApJ, 381, 200